Materials Science Forum
ISSN: 1662-9752, Vol. 1174, pp 9-14
doi:10.4028/p-KbGFC6

Submitted: 2025-07-23
Revised: 2025-09-29
Accepted: 2025-10-28
Online: 2026-01-12

Experimental Studies and Simulation of TRIP-TWIP Roll Bonding

Jennifer Mantel[1,a*], Matthias Schmidtchen[1,b], Mikhail Seleznev[2,c], Anja Weidner[2,d], Horst Biermann[2,e], Ulrich Prahl[1,f]

[1]Institute of Metal Forming, TU Bergakademie Freiberg, Freiberg, 09599, Germany

[2]Institute of Materials Engineering, TU Bergakademie Freiberg, Freiberg, 09599, Germany

[a*]jennifer.mantel@imf.tu-freiberg.de, [b]matthias.schmidtchen@imf.tu-freiberg.de, [c]Mikhail.Seleznev@iwt.tu-freiberg.de, [d]anja.weidner@ww.tu-freiberg.de, [e]biermann@ww.tu-freiberg.de, [f]ulrich.prahl@imf.tu-freiberg.de

Keywords: roll bonding, steel, simulation, TRIP, TWIP.

Abstract. To increase the safety of steels in high performance cases like crash energy absorption, even better properties of the materials are necessary. To advance this research, a TWIP and a TRIP steel were combined in a laminated composite via roll bonding at 450 °C with the goal of using accumulative roll bonding (ARB) in later research to further enhance the properties reaching an ultra-fine-grained material. Two different TWIP layer thicknesses (2 mm and 3 mm) were experimentally roll bonded with a 3 mm thick TRIP layer each using a 4-high rolling mill. A modular Python-based simulation incorporating coupled solving of ordinary differential equations of the temperatures and the horizontal stress changes of the layers were implemented to predict deformation and bonding behavior. Simulated results matched well with experimental data in terms of final geometry and temperature, while roll force deviations indicated the need for the refining of the used model. Furthermore, experimentally asymmetric layer relationships at the beginning and the addition of a thin (10 µm) Ni interlayer were found to enhance bond strength in high-strength steel laminates.

Introduction

High-alloy transformation-induced plasticity (TRIP) and twinning-induced plasticity (TWIP) austenitic stainless steels represent key variants of advanced high-strength steels. TRIP steels exhibit strain-induced martensitic transformation during deformation, which enhances work hardening. TWIP steels, on the other hand, deform primarily through mechanical twinning with both mechanisms leading to a high combination of strength and ductility. [1] To further improve material properties, a severe plastic deformation process like accumulative roll bonding (ARB) can be used, which leads to additional grain refinement in the materials after multiple cycles while retaining the starting geometry with a reduction of 50 %. [2] A laminate combining TRIP and TWIP steels can integrate both deformation mechanisms to improve the overall performance of the material, while also increasing the energy absorption through local deformation in the bonding zone.

Experimental Details:

For this study an X5CrMnNi16-6-6 and an X5CrMnNi16-6-9, respectively steel with a TRIP or a TWIP effect were used. The exact chemical compositions were analyzed by spark emission spectrometry and are given in Table 1.

Table 1. Chemical composition of the TWIP and the TRIP steel, measured by spark emission spectrometry.

Steel	Fe	Cr	Mn	Ni	Si	N	C	Al	Mo	V	Nb
TWIP	Rest	15.8	6.5	9.7	1.00	0.035	0.043	0.001	0.0025	0.01	0.005
TRIP	Rest	15.7	6.7	6.66	0.7	0.035	0.041	0.001	0.0025	0.017	0.005

Both materials were supplied as mold-cast plates by ACtech (Freiberg Germany). Before roll bonding of the two materials, they underwent multiple steps to achieve the desired dimensions and properties, which included annealing, hot rolling and etching. More details can be found in Figure 1.

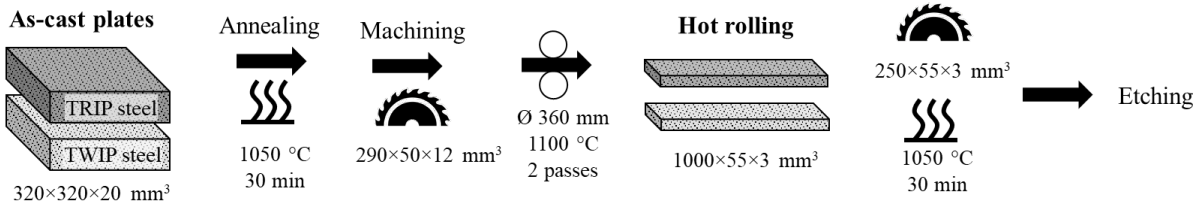

Fig. 1. Production steps before surface treatment and roll bonding of the two materials.

The surface treatment was performed after etching. This process involved degreasing by an acetone-based solvent and shot peening of the bonding interfaces with Al_2O_3 particles using a pressure of 5 bar. The former served to clean the surface and the latter to harden the surface and increase its roughness. Then the materials were stacked and spot welded together at one end.

Rolling was carried out using a reversing rolling mill in a 4-high configuration located at the Institute of Metal Forming (IMF). The radius of the working rolls was 100 mm and the circumferential rolling speed was set to 0.3 m/s. A thickness reduction of 50% per pass was targeted in accordance with the accumulative roll bonding (ARB) process. The entry temperature into the roll gap was maintained at around 450 °C, below the recrystallization temperature of both materials, but sufficiently high to reduce the flow stresses of both materials during deformation and reduce or eliminate the occurrence of the TRIP and TWIP effects during the roll bonding process itself. [3]

Simulation

The simulation model is based on the elementary method of plasticity. In particular for flat rolling, this means that the roll gap is divided into infinitesimal small strips along the rolling direction. An example of a strip element can be seen in Figure 2. This central element is used to describe the state of the materials and the stresses at each point in the roll gap.

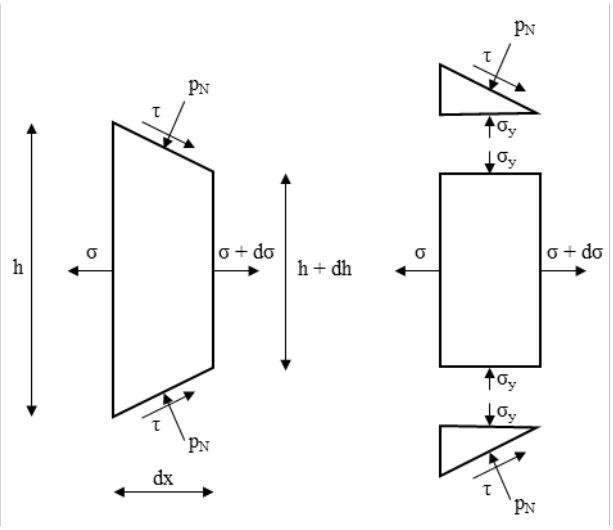

Fig. 2. Strip element according to the elementary method of plasticity.

A custom modular Python program was developed to enable interchangeable sub-models. The core is based on Schmidtchen [4] and assumes a thermal coupled plane strain, rigid-plastic state with strain hardening. Multiple differential equations (ODE) are solved in a coupled state per strip. This includes a separate ODE for the change in the horizontal stress according to Karman [5] for each layer in the unbonded state and afterwards for the complete strip element with a mean flow stress of both layers. In parallel, 1D heat flux calculations for each layer are calculated to include the change in temperature and were adapted from Weiner et al. [6] for multiple layers. In the end,

the simulation performs multiple iterative cycles with the result of fitting the calculated mean horizontal stress to the front tension, which is an input parameter and is zero MPa in all investigated cases. This is done by changing the neutral line for each loop and undergoing the forward calculation from entry to exit of the roll gap.

Due to the incorporated hardening of the materials, a variable layer thickness relationship over the whole gap according to Schmidtchen [4] was used. The roll force and the roll torque are calculated by a piecewise integration over the length of the roll gap, while the roll flattening is solved according to Hitchcock [7], which acts as an outer loop to the coupled solving of the set of ODEs.

Case Study

Two cases were investigated by simulation which have also been realized experimentally.

Case 1: Here, a TWIP steel with an initial height of 2 mm was used, while the TRIP steel had the usual thickness of 3 mm. The other parameters followed the description provided in the experimental details. In the end, the final overall height of 2.33 mm corresponds to a reduction of 53.4 %.

Case 2: In this case, a starting height of 3 mm for each layer was used with a final height of 2.9 mm, therefore a slightly lower reduction of 51.7 % was achieved.

The simulated results can be found in Figure 3 with the dashed blue line representing the TRIP layer and the solid line indicating the TWIP layer. The x-axis is the normalized compressed length of the roll gap with -1.0 indicating the roll gap entry and 0.0 indicating the narrowest point in the roll gap. The dotted vertical line represents the bonding point and the dash-dotted line marks the neutral point.

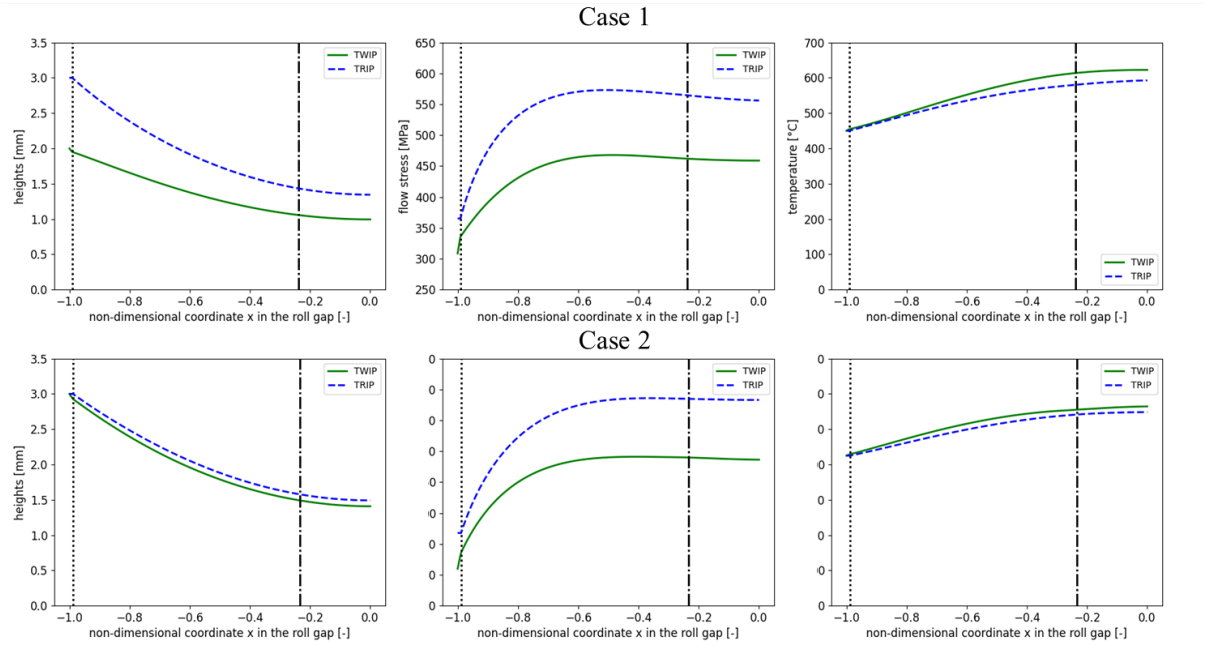

Fig. 3. Simulated curves for the heights (left), flow stresses (middle) and temperatures (right) of the layers with the vertical dotted line indicating the bonding point and the vertical dash-dotted line as the neutral point.

As can be seen, first the height of the softer material (TWIP steel), is reduced until the bonding is initiated while the height of TRIP layer is unchanging. Since the bonding point is relatively close to the roll gap entry, respectively -0.9908 for Case 1 and -0.9885 for Case 2, this zone is short. The bonding point is defined by a fully plastic state in both layers, which means the v.-Mises flow stress criterium for the second layer (TRIP) is fulfilled and the material starts to deform plastically. From this point forward, both layers reduce in height. In the end, for Case 1, the simulated height of the TWIP and TRIP steels, respectively 0.99 and 1.35 mm, matches the final thickness of the materials

(0.90 mm and 1.43 mm) with a deviation of around 0.1 mm for each layer. As for the flow stress of both materials, a similar trend can be seen. This includes that the flow stress of the harder material stays constant before the bonding and then starts to rise. For the calculation, the Freiberg flow stress model [8] was used, which can be seen in Equation 1 with φ_v being the natural logarithm of the mean equivalent strain [-], θ is the temperature in °C, φ'_v equals the mean equivalent strain rate [1/s] and the material dependent coefficients A and m_1 to m_9.

$$k_f = A \cdot e^{(m_1 \cdot \theta)} \cdot \varphi_v^{(m_2)} \cdot e^{(m_4 / \varphi_v)} \cdot (1 + \varphi_v)^{(m_6 + m_5 \cdot \theta)} \cdot e^{(m_7 \cdot \varphi_v)} \cdot \varphi'_v{}^{(m_3 + m_8 \cdot \theta)} \cdot \theta^{(m_9)}. \quad (1)$$

The coefficients were specifically fitted for the two steels according to compression tests carried out between 400 and 700 °C and can be found in Table 2.

Table 2. Freiberg flow stress coefficients for the used TRIP and TWIP steel between 400 and 700 °C.

Coeff.	A	m_1	m_2	m_3	m_4
TWIP	1.17058	-0.00326796	0.392316	-0.0185245	0.00130981
TRIP	0.755002	-0.00359875	0.394698	0.0346997	0.00036809
Coeff.	m_5	m_6	m_7	m_8	m_9
TWIP	-0.0000956118	0	-0.371706	0.000058272	1.27846
TRIP	-0.0000689626	0	-0.365104	-0.00000345044	1.39308

To better compare the simulated with the measured values Table 3 is provided. Due to equipment failure during the roll bonding, the roll force, roll torque and temperatures for Case 1 could not be obtained. Due to the mounting of the pyrometer, only the temperature on the side facing upwards could be measured which was the TRIP side. The simulated end temperature has a negligible difference of 10 K to the measured value.

Table 3. Comparison of measured and simulated roll forces, torques and temperatures.

	Roll Force [kN]		Roll Torque [kNm]		Material	Start/End temperature [°C]	
	measured	simulated	measured	simulated		measured	simulated
Case 1	-	629.9	-	9.18	TWIP	-	450/622.3
					TRIP	-	450/592.6
Case 2	1178	641.0	14.82	10.06	TWIP	-	425/584.4
					TRIP	425/575	425/568

For Case 2, the comparison of the measured and simulated roll force and torque is possible. The measured roll force is significantly higher than the simulated value and while the roll torque fits better, there is still a significant margin left. While the model has been validated by Schmidtchen [4] for other metallic materials, improvement of the model for the current simulation is necessary. For example addressing the spreading and employing a different roll flattening calculation, which is better suited for high roll forces like the model by Fleck and Johnson [9]. Furthermore, microstructural changes were not considered, aside from flow stress curves. Using Equation 2 for the roll force F from Hensel and Spittel [8] with an approximated empirical value of 2.6 for the relationship of the deformation resistance K_{Wm} to the mean flow stress k_{fm} in dependence of the roll gap ratio L_c/h_m according to Equation 3 from Schmidtchen [3], which included the shear stress in roll bonding, it can be shown that the value for the roll force can be estimated to be 1160 kN which fits better with the experimental values. Therefore, shear stress dependency needs to be included in the overall calculation.

$$F = k_{fm} \cdot (K_{Wm}/k_{fm}) \cdot A_c. \quad (2)$$

$$K_{Wm}/k_{fm} = 0.2391\ (L_c/h_m) + 1.4881. \quad (3)$$

K_{wm} is the deformation resistance, k_{fm} is the average flow stress between roll gap entry and roll gap exit, with each of those being the weighted average flow stress over both layers according to the mixture rule at the respective points [Pa], A_c is the compressed area [m^2], which is replaced by the Multiplication of L_c (compressed length, calculated with the flattened radius [m]) with the width of

the stacked materials at the beginning [m]. The weighted average height is calculated according to Equation 4 in [m].

h_m = (starting height of the stack + 2 · final height) / 3. (4)

Concerning the bond strength, it is calculated with the model of Bay and Zhang [10] which includes the surface area enlargement but neglects the surface roughness and its flattening, including the difference of calculating with a nominal flat surface or a rough surface. This leads to the result that the first case has a slightly lower simulated non-dimensional bond strength of 0.66 in comparison to the second case with 0.70. These results are normalized to the starting flow stress of the softer layer. This outcome does not align with experimental observations, where only the sample of Case 1 achieved successful bonding. The maximum of the normal pressure can be found at the neutral point, which is indicated in Figure 3 and is differing by 0.0051 between the two cases (Case 1: -0.2383 and Case 2: -0.2332). Beyond the neutral point, relative movement between the two layers contributes to bond degradation. However, since the displacement is negligible, it does not appear to be the determining factor in the observed difference in experimental bond strength. It is also supported by literature that an asymmetrical set-up is beneficial for bonding in comparison to a symmetrical set-up [11]. This indicated that further investigations into the surface roughness, its effect on bond strength and the inclusion as a simulation model, for example according to Schmidtchen [4], are necessary.

Experimental Results

Challenges arose concerning the bonding of the materials due to the high overall hardness in comparison to usually successfully roll bonded mono materials like Aluminium alloys [12] or to cladding processes where a higher temperature aides the bonding process through diffusion and recrystallization [13]. And while it is possible to bond the chosen materials at the given conditions, as has been shown by Qiu et al. [14] and Seleznev et al. [15], [16], rolling with an intermediate layer has the possibility to enhance the bond strength [10]. This is also supported by experimental results, where an intermediate layer of ultra-high purity (≥ 99.98 %) Ni foil with a starting thickness of 10 µm was used. The bond strength of the samples was investigated by T-peel test according to ASTM-D1876-01 [17]. The maximum peel strength was calculated by dividing the maximum peel strength by the bond width (20 mm) which resulted in a maximum peel strength of 112 N/mm without Ni foil and a value of 250 N/mm with the 10 µm Ni foil. Further investigations into this subject coupled with a simulation of three layers are planned.

Summary

To conclude: the two-layered roll bonding of TWIP on TRIP steel has been investigated by simulation with two different starting thicknesses of the TWIP layer, respectively 2 mm in Case 1 and 3 mm in Case 2 with the same TRIP layer thickness of 3 mm. While the asymmetric case (Case 1) showed better bonding in the experiment, the symmetric case (Case 2) achieved marginally better values in the simulation (non-dimensional difference of 0.04), which indicates a need for improvement of the model, for example through the addition of the surface roughness and its influence on the bonding and the inclusion of the shear stresses in the materials and the bonding zone. On the other hand, end heights and temperatures are aligned well with the experimental results.

Furthermore, introducing a 10 µm Ni intermediate layer yielded promising improvements in maximum peel strength, and related investigations are ongoing.

Acknowledgment

This research was funded by the German Research Foundation (Deutsche Forschungsgemeinschaft (DFG) under grant number 448954974.

References

[1] M. Soleimani, A. Kalhor, and H. Mirzadeh, 'Transformation-induced plasticity (TRIP) in advanced steels: A review', *Mater. Sci. Eng. A*, vol. 795, p. 140023, Sep. 2020, doi: 10.1016/j.msea.2020.140023.

[2] Y. Saito, H. Utsunomiya, N. Tsuji, and T. Sakai, 'Novel ultra-high straining process for bulk materials development of the accumulativer roll bonding (ARB) process', p. 5, 1998.

[3] M. Seleznev, J. Mantel, M. Schmidtchen, U. Prahl, H. Biermann, and A. Weidner, 'Steel–Steel Laminates Manufactured via Accumulative Roll Bonding', *Steel Res. Int.*, vol. 96, no. 5, 2025, doi: https://doi.org/10.1002/srin.202400472.

[4] M. Schmidtchen, *Mehrskalige Modellierung des Walzplattierens und Walzens von Werkstoffverbunden*. in Freiberger Forschungshefte / B, no. 372. Institut für Metallformung, TU Bergakademie Freiberg, 2017.

[5] Th. von Kármán, 'Beitrag zur Theorie des Walzvorganges', *Z. Für Angwandte Math. Mech.*, vol. 5, no. 2, pp. 139–141, 1925, doi: 10.1002/zamm.19250050213.

[6] M. Weiner, M. Schmidtchen, and U. Prahl, 'Extension of the Freiberg layer model by means of elastic-plastic material behavior', *Steel Res. Int.*, 2021, doi: 10.1002/srin.202100373.

[7] J. H. Hitchcock and W. Trinks, 'Roll neck bearings', ASME, New York, Report of Special Research Committee on Roll Neck Bearings, 1935.

[8] A. Hensel and T. Spittel, *Kraft- und Arbeitsbedarf bildsamer Formgebungsverfahren*. Leipzig: VEB Deutscher Verlag für Grundstoffindustrie, 1978.

[9] N. A. Fleck and K. L. Johnson, 'Towards a new theory of cold rolling thin foil', *Int J Mech Sci*, 1987.

[10] N. Bay, C. Clemensen, and O. Juelstorp, 'Bond Strength in Cold Roll Bonding', *Ann. CIRP*, vol. 34, no. 1, 1985.

[11] X. Li, G. Zu, M. Ding, Y. Mu, and P. Wang, 'Interfacial microstructure and mechanical properties of Cu/Al clad sheet fabricated by asymmetrical roll bonding and annealing', *Mater. Sci. Eng. A*, vol. 529, pp. 485–491, Nov. 2011, doi: 10.1016/j.msea.2011.09.087.

[12] P. Chekhonin *et al.*, 'Confined recrystallization of high-purity aluminium during accumulative roll bonding of aluminium laminates', *Acta Mater.*, vol. 60, no. 11, pp. 4661–4671, Jun. 2012, doi: 10.1016/j.actamat.2012.04.004.

[13] O. Bouaziz, J. P. Masse, G. Petitgand, and M. X. Huang, 'A Novel Strong and Ductile TWIP/Martensite Steel Composite', *Adv. Eng. Mater.*, vol. 18, no. 1, pp. 56–59, Jan. 2016, doi: 10.1002/adem.201500113.

[14] Y. Qiu, N. Kaden, M. Schmidtchen, U. Prahl, H. Biermann, and A. Weidner, 'Laminated TRIP/TWIP Steel Composites Produced by Roll Bonding', *Metals*, vol. 9, no. 2, p. 195, Feb. 2019, doi: 10.3390/met9020195.

[15] M. Seleznev, C. Renzing, M. Schmidtchen, U. Prahl, H. Biermann, and A. Weidner, 'Deformation lenses in a bonding zone of high-alloyed steel laminates manufactured by cold roll bonding', *Metals*, Apr. 2022.

[16] M. Seleznev *et al.*, 'Microstructural evolution of the bonding zone in TRIP-TWIP laminate produced by accumulative roll bonding', *Mater. Sci. Eng. A*, Feb. 2022, doi: 10.1016/j.msea.2022.142866.

[17] D14 Committee, *ASTM - D1876-08 - Test Method for Peel Resistance of Adhesives (T-Peel Test)*, West Conshohocken, PA. doi: 10.1520/d1876-08r23.

The publication of this article was funded by the TU Bergakademie Freiberg 10.13039/501100021786